Cancer Research

DNA–SWCNT Biosensors Allow Real-Time Monitoring of Therapeutic Responses in Pancreatic Ductal Adenocarcinoma

Santanu Bhattacharya[1,2], Xun Gong[3], Enfeng Wang[1], Shamit K. Dutta[1], Joseph R. Caplette[2], Manki Son[3], Freddy T. Nguyen[3], Michael S. Strano[3], and Debabrata Mukhopadhyay[1,2]

Abstract

Pancreatic ductal adenocarcinoma (PDAC) is a highly desmoplastic cancer with limited treatment options. There is an urgent need for tools that monitor therapeutic responses in real time. Drugs such as gemcitabine and irinotecan elicit their therapeutic effect in cancer cells by producing hydrogen peroxide (H_2O_2). In this study, specific DNA-wrapped single-walled carbon nanotubes (SWCNT), which precisely monitor H_2O_2, were used to determine the therapeutic response of PDAC cells *in vitro* and tumors *in vivo*. Drug therapeutic efficacy was evaluated *in vitro* by monitoring H_2O_2 differences *in situ* using reversible alteration of Raman G-bands from the nanotubes. Implantation of the DNA–SWCNT probe inside the PDAC tumor resulted in approximately 50% reduction of Raman G-band intensity when treated with gemcitabine versus the pretreated tumor; the Raman G-band intensity reversed to its pretreatment level upon treatment withdrawal. In summary, using highly specific and sensitive DNA-SWCNT nanosensors, which can determine dynamic alteration of hydrogen peroxide in tumor, can evaluate the effectiveness of chemotherapeutics.

Significance: A novel biosensor is used to detect intratumoral hydrogen peroxide, allowing real-time monitoring of responses to chemotherapeutic drugs.

Introduction

Pancreatic ductal adenocarcinoma (PDAC) is the third leading cause of cancer-related deaths in the United States, with a 5-year survival rate of less than 8% (1). PDACs are often diagnosed at a late stage and are unresectable with desmoplastic tumor microenvironments (TME) and show chemoresistance (2–5). Gemcitabine with Abraxane (6) or FOLFIRINOX (a combination of leucovorin, 5-fluorouracil, irinotecan, and oxaliplatin; ref. 7) is the only first-line treatment for PDACs. One major clinical challenge in the chemotherapy is the lack of methods available to monitor therapeutic efficacy in real time. Clinicians are waiting for drugs that can produce significant effects so that the measurable tumor size or metabolism changes can be monitored via expensive imaging techniques such as positron emission tomography–MRI (8). In reality, the complex nature of the genetic makeup of the disease often determines the tumor's resistance to chemotherapy, and the entire duration of treatment will be lost due to the lack of an available *in situ* monitoring system. Hence, the assessment of real-time therapeutic response for better clinical decision-making to treat patients with cancer, in particular those with PDAC, is an unmet clinical need.

Integration of nanotechnology in medicine has successfully demonstrated unprecedented achievements in developing novel therapeutics and diagnostics. As biosensors, single-walled carbon nanotubes (SWCNT) hold great promise for detecting key biological analytes, including nitric oxide (NO), glucose, hydrogen peroxide (H_2O_2), and several others (9–16), compared with other nanostructures, such as solid-state nanopores (17) and nanochannels (18). DNA–SWCNT conjugates are able to demonstrate DNA sequence–dependent molecular recognition. For example, (AT)15-wrapped SWCNTs perform as specific NO sensors (14, 16) and (GT)15-wrapped SWCNTs as H_2O_2 sensors in the biological system (10, 12). SWCNTs exhibit characteristic Raman and photoluminescence (PL) properties in the near-infrared (NIR) spectral region; these properties make them suitable candidates for bioimaging, as most of the biological sample has minimal optical scattering and absorption in the NIR range (700 nm–2,500 nm; ref. 19). Earlier, Heller and colleagues and Jin and colleagues (10, 12) demonstrated that the single-stranded DNA (GT)15 wrapped around the SWCNT surface is highly selective to measure the presence of H_2O_2 with single-molecule sensitivity and high spatial and temporal resolution from cells. These SWCNTs wrapped with (GT)15 exhibit quenching of fluorescence upon exposure to H_2O_2 (12). In addition, SWCNT's Raman signals have been utilized for tissue labeling (20, 21) as well as sensor applications (22, 23).

In cellular and preclinical experiments with small animals, several reports suggest that drugs such as vitamin C (or ascorbate; refs. 24, 25) and gemcitabine (24, 25) induce production of

[1]Department of Biochemistry and Molecular Biology, Mayo Clinic College of Medicine and Science, Jacksonville, Florida. [2]Department of Physiology and Biomedical Engineering, Mayo Clinic College of Medicine and Science, Jacksonville, Florida. [3]Department of Chemical Engineering, Massachusetts Institute of Technology, Cambridge, Massachusetts.

Note: Supplementary data for this article are available at Cancer Research Online (http://cancerres.aacrjournals.org/).

Corresponding Author: Debabrata Mukhopadhyay, Mayo Clinic College of Medicine and Science, 4500 San Pablo Road S, Jacksonville, FL 32224. Phone: 904-953-6177; Fax: 904-953-0277; E-mail: mukhopadhyay.debabrata@mayo.edu

AACR 4515

H_2O_2 (26) within cancer cells during their cytotoxic activity. It is also evident that other routinely used anticancer therapeutics, such as paclitaxel, cisplatin, arsenic trioxide, etoposide, and doxorubicin, likewise increase production of intracellular H_2O_2 in their cytotoxic activity (27–34). Hence, our hypothesis was to develop a minimally invasive, real time, *in vivo* sensor-imaging platform to directly assess the status of the posttreatment tumor and its microenvironment, which can serve as an indicator of therapeutic efficacy. We predict that if gemcitabine is effective, there will be a corresponding production of H_2O_2 in the TME that suggests an effective response from the drug. Thus, if the designed sensor system can monitor the difference in H_2O_2 production in response to gemcitabine treatment, we can correlate the drug response to the tumor cell's cytotoxicity in real time.

Herein, we report on the SWCNT nanosensors' ability to specifically monitor H_2O_2 to evaluate chemotherapeutic response both *in vitro* and *in vivo*. In summary, the DNA–SWCNT hybrids display reversible alternation in Raman and PL properties with dynamic status of endogenous and/or exogenous H_2O_2. Production of intracellular H_2O_2 is correlated with cellular cytotoxicity induced by chemotherapeutics, such as gemcitabine and irinotecan. We observe both Raman and PL signals of SWCNTs in response to the alteration of H_2O_2 *in vitro*. To demonstrate the application of this biosensor as a real-time monitoring platform, we designed a longitudinal study in a PDAC murine model, where this probe successfully recorded the release of H_2O_2 in response to gemcitabine treatment. We also monitored that the Raman signals of SWCNTs revert to the initial pretreatment levels upon withdrawal of treatment, indicating inhibition of exogenous H_2O_2 production. Together with these observations, SWCNTs may be considered as a clinical tool to predict therapeutic outcome.

Materials and Methods

Materials

For our study, we used raw HiPco SWCNTs (batch HR29-039; NanoIntegris Inc.), containing a distribution of small-diameter SWCNTs, DMEM (Corning Incorporated), FBS (Gibco), penicillin–streptomycin (Gibco), PBS (Life Technologies), gemcitabine (Sagent Pharmaceuticals, Inc.), irinotecan (LC Laboratories), CellTiter 96 AQueous One Solution Cell Proliferation Assay (Promega Corporation), 6-carboxy-2′,7′-dichlorodihydrofluorescein diacetate (catalog no. C2938; from Invitrogen), and 0.9% NaCl (AddiPak).

Synthesis of DNA–SWCNT hybrid

(GT)15-SSDNA (IDT) and SWCNT were mixed in a 1 mg to 1 mg weight ratio in 1 mL of 0.1 mol/L NaCl. The mixture was chilled on ice and probe-tip sonicated (Qsonica Q125) with a 1/4-inch tip at 40% amplitude for 30 minutes. The dispersion was then centrifuged twice for 90 minutes at $16,100 \times g$ to remove large particulates, undispersed SWCNTs, and other residual impurities. The absorption spectra of SWCNT dispersions were collected (Cary 5000, Agilent Technologies) and concentrations approximated using the absorbance at 632 nm with an extinction coefficient of 0.036 mg/$(L^{*}cm)^{-1}$ (35).

Cell culture

PANC1 (item number CRL-1469 and batch number 62278038; ATCC) was cultured following a standard method, as described previously (36). Briefly, PANC1 was grown in DMEM supplemented with 10% FBS and 1% penicillin–streptomycin. Cells were thoroughly washed with PBS before any treatment mentioned in the study. For treatment, SWCNT, gemcitabine, and irinotecan were dissolved in supplemented cultured media.

Cell viability assay

For cell viability assay, approximately 5×10^3 cells were plated in 96-well plates and treated with gemcitabine and irinotecan. After 24 and 48 hours of treatment, cells were washed thoroughly with PBS three times. As per the manufacturer's protocol, cells were incubated with 100-μL media containing 20 μL One Solution reagents at 37°C for 30 minutes, and absorbance at 492 nm was measured using SpectraMax i3x (Molecular Devices, LLC).

In vivo tumor growth

All animal studies were performed as per procedures approved by the Mayo Clinic Institutional Animal Care and Use Committee. Orthotopic pancreatic cancer xenograft was developed in 6- to 8-week-old female SCID mice that were obtained from the National Cancer Institute and housed in the institutional animal facilities. SCID mice were anesthetized with ketamine/xylazine prior to any surgical procedures. Effective anesthesia was tested by squeezing the rear paw or pinching the tail to test for reactions. Approximately 1×10^6 PANC1 cells suspended in 50-μL PBS were injected orthotopically into the pancreases of the mice. Tumors were allowed to grow for three weeks. Once the tumor size was approximately 1 cm, tumor-bearing mice were prepared for the longitudinal therapeutic study. Prior to imaging, surgery was performed on each mouse to access the tumor. After anesthesia, the region of interest was sterilized with an iodine solution and a transverse incision was made with scissors at the site of previous surgery to access the pancreatic tumor for imaging. After imaging, the peritoneal membrane and outer incision were sutured as separate layers with surgical absorbable suture, Vicryl 4-0 (undyed, braided).

SWCNT characterization

An NS3 NanoSpectralyzer (Applied NanoFluorescence, LLC) was used for all cuvette-based spectroscopy. We used an InGaAs (Renishaw plc) detector for our study. A 532 nm laser and a 671 nm laser were used for the collection of PL and Raman signals, respectively, from SWCNTs. We used the inVia confocal Raman microscope (Renishaw plc), which was also equipped to record PL spectra and Raman spectra. For live cells and live animal imaging, we used a 785 nm laser with output power of 300 mW and CCD detector (Renishaw plc). For *in vitro* imaging, we used a 40× water immersion lens from Olympus and 1,200 l/mm gratings (Renishaw plc), and for *in vivo* imaging we used 5× air objectives from Leica and 600 l/mm gratings (Renishaw plc). The absorption spectra of (GT)15-wrapped SWCNTs in the presence or absence of H_2O_2, fluorescence excitation–emission, and Raman spectra are presented in Supplementary Figs. S1–S4, respectively.

SWCNT size distribution was measured via NanoSight LM10 (Malvern Panalytical Ltd). Particles were tracked using forward scattered 405 nm laser light, a 10× objective lens, and a CMOS camera. Experiments were performed at 293 K; 30 videos of 30 seconds each were taken and processed with a recently developed Bayesian algorithm to estimate the hydrodynamic radius distribution of the particle population using Matlab and NanoSight NTA 3.2 software (Supplementary Fig. S5).

Transmission electron microscope

After treatment, PANC1 cells were fixed in an electron microscope fixative (4% paraformaldehyde with 1% glutaraldehyde in PBS, pH 7.2), and placed into 2% low-melting agar. Cells were then stained with 1% osmium tetroxide and 2% uranyl acetate, dehydrated through an ethanol series, and embedded into Spurr resin. After a 24-hour polymerization at 60°C, 0.1-μm ultrathin sections were poststained with lead citrate. Micrographs were acquired using a JEOL1400 transmission electron microscope equipped with a Gatan Orius camera (Gatan, Inc.), operating at 80 kV.

Statistical analysis

The data are represented as mean ± SD. All *in vitro* experiments were conducted independently in triplicate. Comparisons between treatment groups were done by Student *t* test. Statistical analysis was conducted with either Microsoft Excel or Origin Labs. $P < 0.05$ was considered statistically significant.

Results

Raman and PL response of DNA–SWCNT hybrid subjected to H_2O_2

In this study, we introduced a wide range of concentrations, from 5 to 200 μmol/L of H_2O_2 to SWCNT suspension (10 μg/mL), transferring the mixture in a quartz cuvette with path length of 1 cm [see Supplementary Materials for (GT)15–SWCNT absorbance, fluorescence, Raman, and size distribution characterization; Supplementary Figs. S1–S5]. The PL and Raman responses of these nanotubes were collected by an NS3 NanoSpectralyzer spectrometer. As illustrated in Fig. 1A, the PL intensity decreased monotonically with increasing concentrations of H_2O_2, as reported previously (10, 12). The PL quenching gradually slowed until 200 μmol/L H_2O_2 reaching a total response of 26% (Fig. 1B). We also monitored similar modulation of the resonance Raman vibrational spectra of SWCNTs as illustrated in Fig. 1C and D.

Detection of chemotherapeutic-induced H_2O_2 using DNA–SWCNT hybrid

Gemcitabine (2′,2′-difluoro-2′-deoxycytidine; dFdC) is a deoxycytidine analogue known to be phosphorylated in the cytoplasm to produce gemcitabine triphosphate within the cells. This metabolite then inhibits DNA synthesis (37), leading to cellular stress and H_2O_2 production (38), followed by induction of apoptosis and cell death (39). To evaluate whether the production of H_2O_2 could be monitored by SWCNT, we used PANC1, a pancreatic cancer cell line. SWCNT (10 μg/mL) was preincubated overnight in PANC1 cells, which were further treated with 10 μmol/L gemcitabine for 12, 24, and 48 hours. Cells were thoroughly washed with PBS and harvested at each time point, followed by sonication, and then PL measurement was conducted via the NanoSpectralyzer (Fig. 2A).

For comparison, we also used commercially available 6-carboxy-2′,7′-dichlorodihydrofluorescein diacetate (carboxy-H2DCFDA) to monitor intracellular H_2O_2 upon gemcitabine treatment. PANC1 cells were cultured in 96-well plates, and then treated with 10 μmol/L gemcitabine for 12, 24, and 48 hours. At each time point, cells were washed three times with PBS and incubated with 10 μmol/L carboxy-H2DCFDA. After 1 hour, green fluorescence was recorded using a SpectraMax i3X plate reader from each well of the plate to measure the H_2O_2. Both carboxy-

H2DCFDA and SWCNT biosensor showed a similar trend in monitoring H_2O_2 production with respect to the different time points of gemcitabine treatment, but the relative sensitivity for the SWCNT sensors was superior to that of the carboxy-H2DCFDA (Fig. 2A). The relative sensitivity was determined using the following equation:

$$\Delta PL = 1 - \frac{I}{I_0} \qquad (A)$$

I is the PL intensity from gemcitabine-treated cells at any time point and I_0 is the PL intensity from cells without treatment. We also performed an *in vitro* cell viability assay to measure the fate of the cells after exposure to 10 μmol/L gemcitabine at 24- and 48-hour time points using the same 96-well experimental setup used for carboxy-H2DCFDA. Percentage viability was calculated using the following equation:

$$Viability\% = 100 \times \frac{Abs_{Treated} - Abs_{Blank}}{Abs_{Untreated} - Abs_{Blank}} \qquad (B)$$

Abs represents the absorption. Results presented in Fig. 2B clearly demonstrate that with time, cell viability significantly diminished. Hence, we found a direct correlation of cell viability with H_2O_2 production due to gemcitabine treatment as reported previously (26).

Live cell Raman microscopy provides spatial distribution of chemotherapy-induced H_2O_2

We further employed live cell imaging to understand the spatial distribution of H_2O_2 production. PANC1 was cultured in a quartz bottom 50-mm Petri dish and then incubated with the SWCNT biosensor at a final concentration of 10 μg/mL in cell culture media overnight. After thorough washing with PBS three times, the cells were treated with two different concentrations of gemcitabine, 5 and 10 μmol/L, for 72 hours. Finally, the cells were washed and prepared for live cell imaging using a Renishaw inVia confocal microscope. Before each measurement with the instrument, the Raman signal was calibrated with a silicon substrate. Using line scan with 15 mW laser power and 1 second exposure time, Raman spectra were collected from individual points of a line arbitrarily drawn over the cells; each point was separated by 1 μm and the line consisted of 53 such points over the live cells. These points were overlaid on the bright-field image of the corresponding cell as illustrated in Fig. 3A. The inset of Fig. 3A shows the Raman spectrum collected from one such point and confirms the presence of SWCNT within the cell. The Raman G-band intensity at 1,590 cm^{-1} corresponding to each data point was then overlaid on the white light image. From the spectral signatures, we can specifically monitor the spatial distribution of SWCNTs within the cells. The laser power was optimized prior to the experiment to prevent any detrimental effect on the live cells. Furthermore, these spectra were collected using confocal mode to minimize the influence of Raman signals from surrounding SWCNTs. The intracellular spatial variation of the Raman spectra is presented in Fig. 3B. In the selected NIR excitation wavelength (785 nm), no significant autofluorescence interference from cellular components was detected. Figure 3C and D displays the Raman signals from cells treated with 5 and 10 μmol/L gemcitabine for 72 hours, respectively. As evident from the morphology of the cells, gemcitabine was effectively toxic (Fig. 3C and D). The vertical color bar in Fig. 3A, C, and D indicates the range of intensity corresponding to the characteristic Raman peak G-band
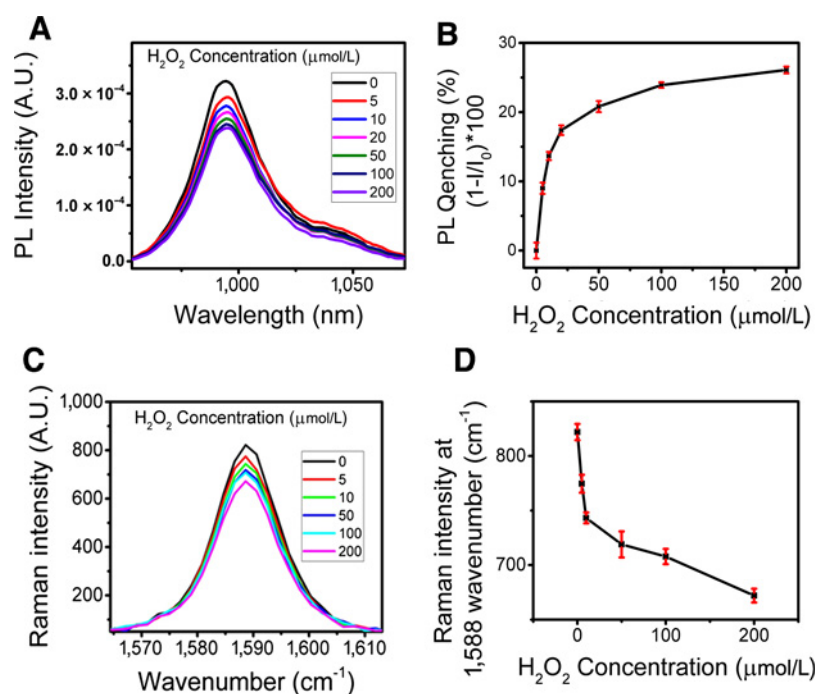
Bhattacharya et al.

Figure 1.
Detection of H_2O_2 using DNA–SWCNT hybrid. **A,** Photoluminescence spectra obtained from SWCNT (10 µg/mL) after incubation with H_2O_2 concentrations from 0 to 200 µmol/L. **B,** Percentage of PL quenching has been plotted with concentration of H_2O_2. **C,** Raman spectra collected from SWCNT after incubation with H_2O_2 concentrations from 0 to 200 µmol/L. **D,** Raman intensity corresponding to G-band was plotted with concentration of H_2O_2.
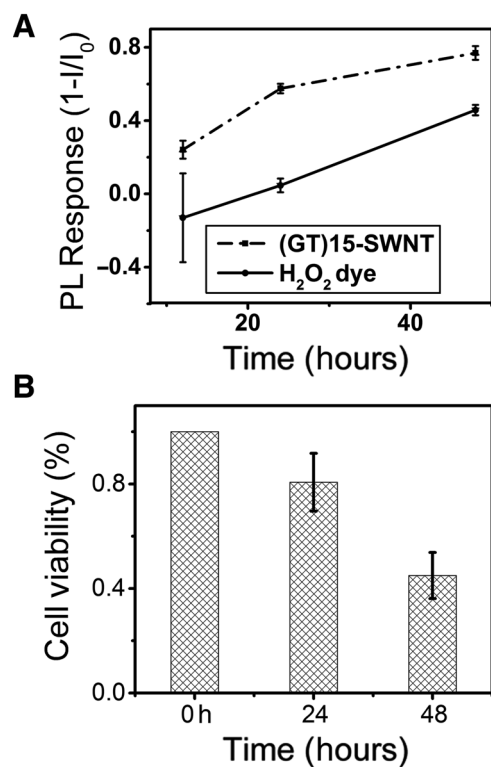
Figure 2.
Detection of H_2O_2 in gemcitabine-treated cancer cell and cytotoxicity study. **A,** Endogenous expression of H_2O_2 measured using PL signals corresponding to carboxy-H2DCFDA and SWCNT biosensor. **B,** Cell viability assay of PANC1 after exposure to 10 µmol/L gemcitabine at three different time points.

of SWCNTs in untreated and treated cells, respectively, and the significant reduction in the maximum intensity range correlates to the Raman signal decrease due to the presence of intracellular H_2O_2. For treated cells, with increasing concentrations of gemcitabine, more attenuation of the Raman signal was observed inside the PANC1 cells as summarized in Fig. 3E and F. Figure 3E represents the spatial distribution of Raman signals and Fig. 3F displays a bar graph to present variation in maximum intensity subject to gemcitabine exposure. These data support the current literature, where it has been shown that a higher concentration of gemcitabine results in increased H_2O_2 production (38), and hence, we found more attenuation in Raman signals of SWCNTs. The cell viability assay also confirmed the toxicity from gemcitabine at 5 and 10 µmol/L concentrations after 72 hours of exposure (Fig. 3G). It is evident from Figures 3A, C, and D that there are spatial variations of H_2O_2 production inside the cells that display a varying amount of Raman signal modulation in SWCNTs. Gemcitabine triphosphate, not the gemcitabine itself, binds to the DNA inside the cells (40). To illustrate that the gemcitabine itself is not contributing to SWCNT's PL quenching by binding with (GT)15 present on the surface of SWCNTs, we incubated gemcitabine with SWCNT biosensors for 72 hours. PL spectra from these samples were collected by the NanoSpectralyzer as presented in Fig. 3H. No variation was observed in the PL intensity of signature peaks corresponding to SWCNTs in the presence of gemcitabine, suggesting that gemcitabine itself has no nonspecific contribution to the PL response. We did not observe any significant alteration in PL spectra collected from SWCNTs incubated in PANC1 cells up to 72 hours (Supplementary Fig. S6).

Furthermore, we have incorporated another chemotherapeutic drug, irinotecan, which showed similar results (Fig. 4). After overnight preincubation with SWCNT, PANC1 cells were exposed to 120 µmol/L irinotecan for 72 hours. Cells were thoroughly washed with PBS before imaging. In Fig. 4A, SWCNT displays a similar Raman response to that in Fig. 3A. After 120 µmol/L

Figure 3.
Monitoring spatial distribution of H_2O_2 with varying concentrations of gemcitabine. **A,** PANC1 treated with SWCNTs. Raman spectra were collected from each point on the dotted line. The color map on the dotted line is based on intensity at 1,590 cm^{-1}. One such spectrum is shown in the inset and the corresponding point in the line scan is identified by the arrow sign. The color bar displays the range of Raman signals recorded in an individual image. **B,** Spectra collected from each point was plotted in a 3D graph, where the x-axis represents the wave number (cm^{-1}), the y-axis represents the coordinate of the line, and the z-axis represents the intensity in arbitrary units. **C,** A representative picture of the line scan on cells after treatment with 5 µmol/L gemcitabine. The color bar displays the range of Raman signals recorded in each individual image. **D,** A representative picture of line scan on cells after treatment with 10 µmol/L gemcitabine. The color bar displays the range of Raman signals recorded in each individual image. **E,** 3D representation of intensity profile from **A**, **C**, and **D**, demonstrating effective decrease of Raman signals with increasing doses of GEM in vitro. The dataset is presented with offset on the x-axis to demonstrate its intensity profile without overlapping. **F,** Bar graph representing alteration of the maximum intensity of Raman signals with increasing concentrations of gemcitabine. ****, P < 0.0001. **G,** Cell viability assay of PANC1 after exposure of 5 µmol/L and 10 µmol/L gemcitabine for 72 hours. **H,** PL spectra obtained from SWCNT incubation with (red line) or without (black line) gemcitabine. Both spectra overlap showing no effective influence of gemcitabine on PL spectra of SWCNTs.
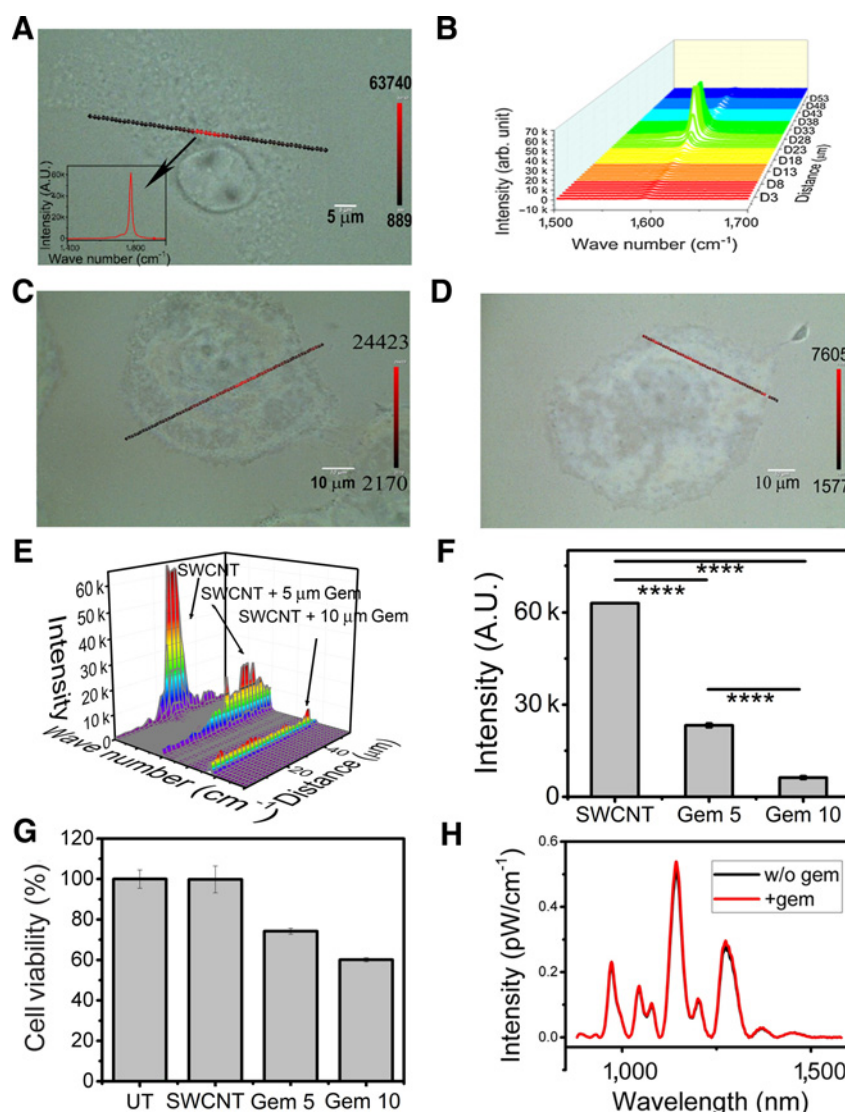
irinotecan treatment, around 50% Raman signal change was monitored (as displayed in Fig. 4B by the color scale) due to the production of intracellular H_2O_2 from treatment. These observations were very consistent throughout the cell culture dish for both gemcitabine and irinotecan treatments (Supplementary Fig. S7). Figure 4C demonstrates the spatial distribution of Raman G-band signals over the line scan. The cell viability assay confirms that irinotecan at 120 µmol/L concentration delivers significant cytotoxicity to PANC1 cells after 72 hours of exposure (Fig. 4D). Figure 4E summarizes the effect on the spatial distribution of Raman G-band signals from 120 µmol/L irinotecan treatment, which directly correlates with the level of intracellular H_2O_2. Figure 4F demonstrates the quantitative analysis of the results presented in Supplementary Fig. S7. To verify endocytosis of SWCNTs, we have performed TEM analysis as shown in Supplementary Fig. S8.

In vivo Raman imaging and assessment of real-time chemotherapeutic outcome of pancreatic cancer in a longitudinal mice model

We also present a longitudinal study of H_2O_2 sensing in an in vivo animal model by monitoring the dynamic status of H_2O_2

inside the tumor of a live animal through (GT)15-wrapped SWCNT following gemcitabine treatment. Briefly, every mouse underwent three survival surgeries during the study and was imaged three times. Orthotopic pancreatic cancer xenograft was developed at the first survival surgery. After the tumor size reached approximately 1 cm, the second survival surgery was executed to implant SWCNT sensors in the tumor. A small well was made in the tumor using a puncher, and then 20 µL of SWCNT probe was delivered in the well and secured in the tumor using biological glue. The dry spot from the biological glue was later used to locate the sensor implantation site. Using a Renishaw inVia confocal microscope, we first assessed the optical slice with maximum intensity profile using a 785 nm laser at 30 mW power (1-second exposure), and Raman spectra were collected using 600 l/mm grating and a Renishaw CCD detector. The selection of an NIR laser allowed us to perform deep-tissue imaging in our study. Nominal laser power was used to avoid tissue damage. We performed a depth profile, where Raman spectra were collected from different tumor depths, surface to 2,000 µm deep, with a 200 µm interval in the longitudinal direction (Fig. 5). This depth analysis confirmed that SWCNTs located approximately 200 µm

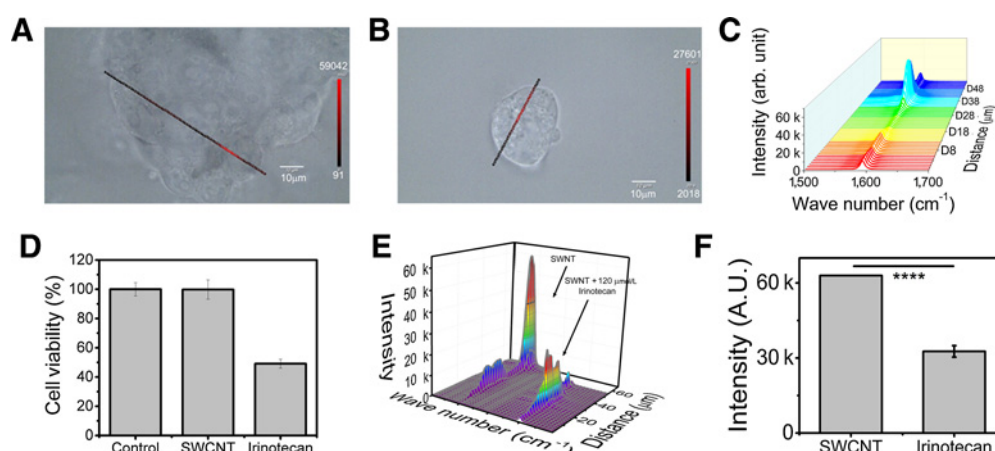**Figure 4.**
Detection of H_2O_2 and its spatial distribution in irinotecan-treated cancer cell. PANC1 cells incubated with 10 μg/mL SWCNTs overnight, followed by irinotecan treatment for 72 hours. Cell without irinotecan treatment (**A**) and cell with 120 μmol/L irinotecan treatment (**B**). The color bar displays the range of Raman signals recorded in an individual image. **C,** Spectra collected from each point have been plotted in a 3D graph, where the *x*-axis represents the wave number (cm^{-1}), the *y*-axis represents the coordinate of the line, and the *z*-axis represents the intensity in arbitrary units. **D,** Cell viability assay of PANC1 after incubation with 120 μmol/L irinotecan for 72 hours. **E,** 3D representation of intensity profile from **A** and **B** demonstrating decrease of Raman signals with irinotecan treatment *in vitro*. The dataset is presented with offset on the *x*-axis to demonstrate its intensity profile without overlapping. **F,** Maximum Raman intensity presented in the bar graph displays the effect of irinotecan treatment on H_2O_2 production. ****, $P < 0.0001$.

below the surface produced maximum Raman signals. Then, we performed an area scan surrounding the implanted site at a depth where maximum Raman signals of SWCNTs were acquired (~200 μm) in all mice. The separation between points in the area map was 20 μm in both lateral directions. To maintain mice hydration, all mice received sterile 0.9% NaCl prior to live imaging and lubricant eye drops from Refresh Plus (Allergan, Inc.) during imaging. These mice were maintained under mild anesthesia using a continuous flow of 1% to 2% isoflurane and placed on heating stage set to 37°C. After imaging, the peritoneal membrane and outer incision were sutured as separate layers with surgical absorbable suture, Vicryl 4-0. The G-band peaks at 1,590 cm^{-1} of SWCNTs were monitored in these spectra. A typical map is presented in Fig. 6A using the intensity profile at 1,590 cm^{-1}. It has been previously described that cancer cells produce H_2O_2 at a basal level (41). Hence, the recorded Raman signal from

implanted SWCNTs (Fig. 6A) was considered the basal level of H_2O_2 in the TME.

One day after the second survival surgery, each mouse was treated with a 40 mg/kg dose of gemcitabine for three days (42). In agreement with previous studies from our laboratory and others, gemcitabine at this dose was effective enough and started killing the tumor cells *in vivo*, hence predicting elevation of the H_2O_2 level in the TME (43). Hence, we performed the third survival surgery to assess whether the nanosensors were able to detect the change of H_2O_2 production in the TME after gemcitabine treatment in live mice. The surgery was done on the microscope stage and anesthesia was maintained with a continuous flow of isoflurane. For imaging, the same experimental parameters were used as mentioned earlier for live mouse imaging. The biological glue used previously for securing SWCNTs within the tumor was spotted, and the scanning area was determined. The optical plane for area scan was again determined by performing a depth scan in each mouse to obtain maximum Raman signals from SWCNTs. The characteristic G-band of SWCNTs was noticed in the Raman spectra obtained from the area scan from the live animal, though the intensity of these peaks was significantly reduced, as evident from the color map scale in Fig. 6B. This Raman signal change can be attributed to the production of H_2O_2 at an elevated level in the tumor microenvironment due to gemcitabine treatment.

The plasma half-life for gemcitabine is approximately 0.28 hour in mice (44). To examine whether withdrawal of gemcitabine treatment could revert the H_2O_2 in the TME to its pretreatment levels, we kept each mouse alive for two more weeks without any further treatment. Mice were then sacrificed and tumor mass was scanned at the same area specified by the biological glue. We performed another depth scan to optimize the optical plane with maximum Raman signals from SWCNTs and performed an area scan thereafter. The Raman signal in each mouse was found to be almost similar to its corresponding pretreatment level, as presented by the color map scale in Fig. 6C. The reduced spatial distribution in Fig. 6C may be due to the orientation of the mouse
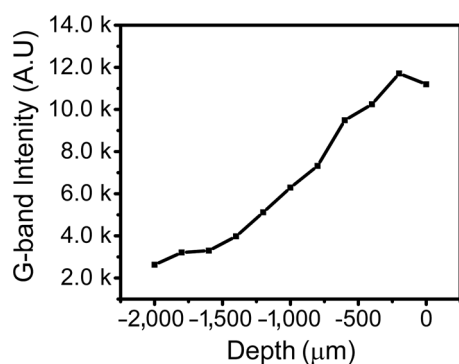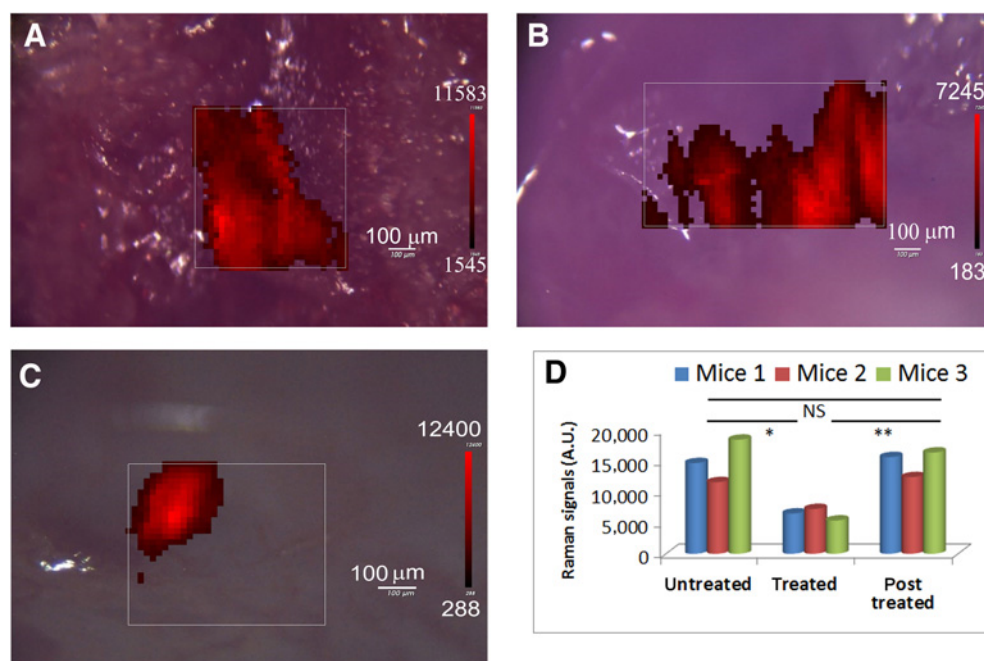

Figure 5.
Depth profile of Raman G-band intensity. The tumor was scanned in the longitudinal direction to find the depth corresponding to maximum Raman signals.

Figure 6.
Longitudinal live animal imaging. Tumor site of the same mice imaged before initiation of treatment (**A**), after three treatments of gemcitabine (**B**), and two weeks after withdrawal of treatment (**C**). The red color map is based on the Raman signals from SWCNTs at 1,590 cm^{-1}. **D,** The maximum level of Raman signals from SWCNTs corresponding to these three distinct treatment conditions is displayed for all three mice. $*$, $P < 0.05$; $**$, $P < 0.01$; NS, nonsignificant.

during imaging. Pancreatic cancer is characterized by its highly desmoplastic TME, but minimal-diffusion SWCNTs cannot be ignored. We performed an area scan over the tumor cross section and mapped for Raman signals of SWCNTs, confirming the localization and integrity of SWCNTs at the implanted site (Supplementary Fig. S9). In Fig. 6D, we present a comparative analysis of maximum Raman G-band intensities obtained from the above-mentioned longitudinal animal study on three mice. Data corresponding to each individual mouse are displayed by separate colors. It is evident that the signal significantly decreased with gemcitabine treatment in mice compared with both pre- and posttreatment levels. These observations also confirmed that gemcitabine therapy can induce the production of H_2O_2, and upon withdrawal of treatment, the elevated level of H_2O_2 diminished.

Discussion

Chemotherapeutics that show significant cytotoxicity to cancer cells by several key mechanisms often produce oxidative stress in the cell (27–31, 34). Hence, generation of H_2O_2 in these circumstances can be evaluated as a key parameter to estimate the merit of any chemotherapeutics in chemoresistant pancreatic cancer. So far, several fluorophore-based assay systems have been explored to measure the endogenously expressed H_2O_2 (45). Among them, the most commonly used H_2O_2 indicator is carboxy-H2DCFDA, which provides green fluorescence upon exposure to reactive oxygen species (ROS) in cells (46). However, their application in animal studies is very limited due to signal attenuation and autofluorescence of live tissue. To overcome these limitations, a significant effort has been made to develop an H_2O_2 sensor with NIR absorption and fluorescence as tissues are optically transpar-

ent in the NIR spectral window. One such successful nanoplatform is SWCNT, which performs as a highly selective and sensitive H_2O_2 sensor when wrapped with (GT)15 (10, 12).

SWCNTs have been well characterized for their intrinsic NIR fluorescence and Raman spectroscopy. The Raman signal of SWCNT is largely observable due to the phenomenon of resonance Raman scattering (47, 48), where the incident light is near the frequency of the electronic transition of a specific SWCNT chirality, augmenting Raman emissions. SWCNT absorbance decreases with H_2O_2 (Supplementary Fig. S2), which should result in a corresponding decrease in Raman signal. The Raman signature of SWCNT is sensitive to the local environment and has been used for sensor application (23). Because H_2O_2 has a well-documented effect on the strength of the optical absorption transition, and the resonant Raman peak intensities necessarily couple to these transitions, there is a mechanism for detecting H_2O_2 using Raman spectroscopy. This mechanism is the same as what has been previously observed for H^+ (49). It is important to note from excitation–emission maps (Supplementary Fig. S3) that there exists a distribution of SWCNT chiralities as well as a distribution of SWCNT lengths in these sensor solutions. The calibration here relates to the mean population response to H_2O_2 and is applied as such in subsequent sections. It is this modulation of PL and Raman signals, explored extensively in the biological environment (50), that is now applied to the case of chemotherapeutic response.

We have noticed that both PL and Raman signals attenuate monotonically with increasing concentrations of H_2O_2 (Fig. 1). To monitor the influence of chemotherapeutics on the production of H_2O_2, we treated PANC1 cells with both gemcitabine and irinotecan at concentrations that significantly deliver cytotoxicity to PANC1 cells. As shown in Fig. 2, SWCNTs display higher

sensitivity over carboxy-H2DCFDA in the detection of intracellular H_2O_2. Furthermore, study of Raman signal attenuation from SWCNTs illustrates the spatial distribution of H_2O_2 production inside the cells treated with gemcitabine and irinotecan (Figs. 3 and 4).

To understand the dynamic influence of therapeutics by monitoring the resulting variation in H_2O_2 production, we designed a longitudinal study on a PANC1 orthotopic xenograft model in mice. (GT)15-wrapped SWCNTs were implanted in PDAC tumor during a critical survival surgery. The Raman signals were immediately recorded from tissue-embedded SWNCTs and utilized as a reference for further analysis. To identify the optical plane of maximum signals, Raman signals were collected from different depths of tissue (tumor surface was set as origin; Fig. 5). This precautionary exercise was repeated for further measurements. A significant reduction in Raman intensity from SWCNTS was monitored in gemcitabine-treated mice, confirming the elevated level of intratumor H_2O_2 production. Upon recovery from the influence of gemcitabine treatment, H_2O_2 levels returned to normal and Raman signals reached the reference level (Fig. 6).

To the best of our knowledge, there is no report of using an SWCNT-based biosensor, or perhaps any other sensor system, to longitudinally evaluate the chemotherapeutic outcome of any drug in a live animal tumor model, in real time. This assessment of dynamic changes of H_2O_2 in real time and also *in situ* can be employed further to evaluate the efficacy of other drugs in different tumor types.

References

1. Lee SH, Kim OK, Lee S, Kim JK. Local-dependency of morphological and optical properties between breast cancer cell lines. Spectrochim Acta A Mol Biomol Spectrosc 2018;205:132–8.
2. Hamada S, Masamune A, Shimosegawa T. Novel therapeutic strategies targeting tumor-stromal interactions in pancreatic cancer. Front Physiol 2013;4:331.
3. McCarroll JA, Naim S, Sharbeen G, Russia N, Lee J, Kavallaris M, et al. Role of pancreatic stellate cells in chemoresistance in pancreatic cancer. Front Physiol 2014;5:141.
4. Schober M, Jesenofsky R, Faissner R, Weidenauer C, Hagmann W, Michl P, et al. Desmoplasia and chemoresistance in pancreatic cancer. Cancers 2014;6:2137–54.
5. Whatcott CJ, Posner RG, Von Hoff DD, Han H. Desmoplasia and chemoresistance in pancreatic cancer. In:Grippo PJ, Munshi HG, editors. Pancreatic cancer and tumor microenvironment. Trivandrum, India; 2012.
6. Goldstein D, El-Maraghi RH, Hammel P, Heinemann V, Kunzmann V, Sastre J, et al. nab-Paclitaxel plus gemcitabine for metastatic pancreatic cancer: long-term survival from a phase III trial. J Natl Cancer Inst 2015; 107. doi: 10.1093/jnci/dju413.
7. Papadatos-Pastos D, Thillai K, Rabbie R, Ross P, Sarker D. FOLFIRINOX - a new paradigm in the treatment of pancreatic cancer. Expert Rev Anticancer Ther 2014;14:1115–25.
8. Ruf J, Lopez Hänninen E, Böhmig M, Koch I, Denecke T, Plotkin M, et al. Impact of FDG-PET/MRI image fusion on the detection of pancreatic cancer. Pancreatology 2006;6:512–9.
9. Giraldo JP, Landry MP, Kwak SY, Jain RM, Wong MH, Iverson NM, et al. A ratiometric sensor using single chirality near-infrared fluorescent carbon nanotubes: application to *in vivo* monitoring. Small 2015;11:3973–84.
10. Heller DA, Jin H, Martinez BM, Patel D, Miller BM, Yeung T-K, et al. Multimodal optical sensing and analyte specificity using single-walled carbon nanotubes. Nat Nanotechnol 2008;4:114.
11. Iverson NM, Strano MS, Wogan GN. *In vivo* delivery of nitric oxide-sensing, single-walled carbon nanotubes. Curr Protoc Chem Biol 2015;7:93–102.
12. Jin H, Heller DA, Kalbacova M, Kim J-H, Zhang J, Boghossian AA, et al. Detection of single-molecule H2O2 signalling from epidermal growth factor receptor using fluorescent single-walled carbon nanotubes. Nat Nanotechnol 2010;5:302.
13. Kim JH, Heller DA, Jin H, Barone PW, Song C, Zhang J, et al. The rational design of nitric oxide selectivity in single-walled carbon nanotube near-infrared fluorescence sensors for biological detection. Nat Chem 2009;1: 473–81.
14. Ulissi ZW, Sen F, Gong X, Sen S, Iverson N, Boghossian AA, et al. Spatio-temporal intracellular nitric oxide signaling captured using internalized, near-infrared fluorescent carbon nanotube nanosensors. Nano Lett 2014; 14:4887–94.
15. Yum K, McNicholas TP, Mu B, Strano MS. Single-walled carbon nanotube-based near-infrared optical glucose sensors toward *in vivo* continuous glucose monitoring. J Diabetes Sci Technol 2013;7:72–87.
16. Zhang J, Boghossian AA, Barone PW, Rwei A, Kim JH, Lin D, et al. Single molecule detection of nitric oxide enabled by d(AT)15 DNA adsorbed to near infrared fluorescent single-walled carbon nanotubes. J Am Chem Soc 2011;133:567–81.
17. Zhu L, Gu D, Liu Q. Hydrogen peroxide sensing based on inner surfaces modification of solid-state nanopore. Nanoscale Res Lett 2017;12:422.
18. Ali M, Tahir MN, Siwy Z, Neumann R, Tremel W, Ensinger W. Hydrogen peroxide sensing with horseradish peroxidase-modified polymer single conical nanochannels. Anal Chem 2011;83:1673–80.
19. Smith AM, Mancini MC, Nie S. Second window for in vivo imaging. Nat Nanotechnol 2009;4:710–1.
20. Liu Z, Davis C, Cai W, He L, Chen X, Dai H. Circulation and long-term fate of functionalized, biocompatible single-walled carbon nanotubes in mice probed by Raman spectroscopy. Proc Natl Acad Sci U S A 2008; 105:1410.
21. Liu Z, Tabakman S, Sherlock S, Li X, Chen Z, Jiang K, et al. Multiplexed five-color molecular imaging of cancer cells and tumor tissues with carbon nanotube Raman tags in the near-infrared. Nano Res 2010;3:222–33.
22. Zhou Q, Zheng J, Qing Z, Zheng M, Yang J, Yang S, et al. Detection of circulating tumor DNA in human blood via DNA-mediated surface-enhanced Raman spectroscopy of single-walled carbon nanotubes. Anal Chem 2016;88:4759–65.

23. Bansal J, Singh I, Bhatnagar PK, Mathur PC. DNA sequence detection based on Raman spectroscopy using single walled carbon nanotube. J Biosc Bioeng 2013;115:438–41.

24. Polireddy K, Dong R, Reed G, Yu J, Chen P, Williamson S, et al. High dose parenteral ascorbate inhibited pancreatic cancer growth and metastasis: mechanisms and a phase I/IIa study. Sci Rep 2017;7:17188.

25. Cieslak JA, Cullen JJ.Treatment of pancreatic cancer with pharmacological ascorbate. Curr Pharm Biotechnol 2015;16:759–70.

26. Chen S-H, Li D-L, Yang F, Wu Z, Zhao Y-Y, Jiang Y. Gemcitabine-induced pancreatic cancer cell death is associated with MST1/Cyclophilin D mitochondrial complexation. Biochimie 2014;103:71–9.

27. Laurent A, Weill B, Nicco C, Chéreau C, Goldwasser F, Batteux F, et al. Improvement of the therapeutic index of anticancer drugs by the superoxide dismutase mimic mangafodipir. J Nat Cancer Inst 2006;98:236–44.

28. Jing Y, Dai J, Chalmers-Redman RME, Tatton WG, Waxman S. Arsenic trioxide selectively induces acute promyelocytic leukemia cell apoptosis via a hydrogen peroxide-dependent pathway. Blood 1999;94:2102–11.

29. Mizutani H, Tada-Oikawa S, Hiraku Y, Kojima M, Kawanishi S. Mechanism of apoptosis induced by doxorubicin through the generation of hydrogen peroxide. Life Sci 2005;76:1439–53.

30. Wagner BA, Evig CB, Reszka KJ, Buettner GR, Burns CP. Doxorubicin increases intracellular hydrogen peroxide in PC3 prostate cancer cells. Arch Biochem Biophys 2005;440:181–90.

31. Alexandre J, Batteux F, Nicco C, Chéreau C, Laurent A, Guillevin L, et al. Accumulation of hydrogen peroxide is an early and crucial step for paclitaxel-induced cancer cell death both in vitro and in vivo. Internat J Cancer 2006;119:41–8.

32. Kajiwara K, Ikeda K, Kuroi R, Hashimoto R, Tokumaru S, Kojo S. Hydrogen peroxide and hydroxyl radical involvement in the activation of caspase-3 in chemically induced apoptosis of HL-60 cells. Cell Mol Life Sci 2001;58:485–91.

33. Ikeda K, Kajiwara K, Tanabe E, Tokumaru S, Kishida E, Masuzawa Y, et al. Involvement of hydrogen peroxide and hydroxyl radical in chemically induced apoptosis of HL-60 cells. Biochem Pharmacol 1999;57:1361–5.

34. Diaz B, Ostapoff KT, Toombs JE, Lo J, Bonner MY, Curatolo A, et al. Tris DBA palladium is highly effective against growth and metastasis of pancreatic cancer in an orthotopic model. Oncotarget 2016;7:51569–80.

35. Zhang J, Kruss S, Hilmer AJ, Shimizu S, Schmois Z, De La Cruz F, et al. A rapid, direct, quantitative, and label-free detector of cardiac biomarker troponin T using near-infrared fluorescent single-walled carbon nanotube sensors. Adv Healthcare Mater 2014;3:412–23.

36. Pal K, Al-Suraih F, Gonzalez-Rodriguez R, Dutta SK, Wang E, Kwak HS, et al. Multifaceted peptide assisted one-pot synthesis of gold nanoparticles for plectin-1 targeted gemcitabine delivery in pancreatic cancer. Nanoscale 2017;9:15622–34.

37. Huang P, Chubb S, Plunkett W. Action of 2',2'-Difluorodeoxycytidine on DNA Synthesis. Cancer Res 1991;51:6110–7.

38. Chen C, Sun J, Liu G, Chen J. Effect of small interference RNA targeting HIF-1alpha mediated by rAAV combined L: -ascorbate on pancreatic tumors in athymic mice. Pathol Oncol Res 2009;15:109–14.

39. Habiro A, Tanno S, Koizumi K, Izawa T, Nakano Y, Osanai M, et al. Involvement of p38 mitogen-activated protein kinase in gemcitabine-induced apoptosis in human pancreatic cancer cells. Biochem Biophys Res Commun 2004;316:71–7.

40. de Sousa Cavalcante L, Monteiro G. Gemcitabine: Metabolism and molecular mechanisms of action, sensitivity and chemoresistance in pancreatic cancer. Eur J Pharmacol 2014;741:8–16.

41. Lisanti MP, Martinez-Outschoorn UE, Lin Z, Pavlides S, Whitaker-Menezes D, Pestell RG, et al. Hydrogen peroxide fuels aging, inflammation, cancer metabolism and metastasis: The seed and soil also needs "fertilizer". Cell Cycle 2011;10:2440–9.

42. Henderson SE, Ding L-Y, Mo X, Bekaii-Saab T, Kulp SK, Chen C-S, et al. Suppression of tumor growth and muscle wasting in a transgenic mouse model of pancreatic cancer by the novel histone deacetylase inhibitor AR-42. Neoplasia 2016;18:765–74.

43. Donadelli M, Dando I, Zaniboni T, Costanzo C, Dalla Pozza E, Scupoli MT, et al. Gemcitabine/cannabinoid combination triggers autophagy in pancreatic cancer cells through a ROS-mediated mechanism. Cell Death Dis 2011;2:e152.

44. Shipley LA, Brown TJ, Cornpropst JD, Hamilton M, Daniels WD, Culp HW. Metabolism and disposition of gemcitabine, and oncolytic deoxycytidine analog, in mice, rats, and dogs. Drug Metab Disposition 1992;20:849–55.

45. Flávia R, P BR, Katrin S.Detection of hydrogen peroxide with fluorescent dyes. Antioxid Redox Signal 2018;29:585–602.

46. Trayner ID, Rayner AP, Freeman GE, Farzaneh F. Quantitative multiwell myeloid differentiation assay using dichlorodihydrofluorescein diacetate (H2DCF-DA) or dihydrorhodamine 123 (H2R123). J Immunol Methods 1995;186:275–84.

47. Vauthey J-N, Dixon E.AHPBA/SSO/SSAT consensus conference on resectable and borderline resectable pancreatic cancer: rationale and overview of the conference. Ann Surg Oncol 2009;16:1725–6.

48. Smith E, Dent G. Modern Raman spectroscopy—a practical approach. Chichester, United Kingdom: John Wiley and Sons Ltd; 2005. p. 210.

49. Strano MS, Huffman CB, Moore VC, O'Connell MJ, Haroz EH, Hubbard J, et al. Reversible, band-gap-selective protonation of single-walled carbon nanotubes in solution. J Phys Chem B 2003;107:6979–85.

50. Bhattacharya S, Roxbury D, Gong X, Mukhopadhyay D, Jagota A. DNA conjugated SWCNTs enter endothelial cells via Rac1 mediated macropinocytosis. Nano Lett 2012;12:1826–30.